First-Principles Modeling of Electrostatically Doped Perovskite Systems

Massimiliano Stengel*

Institut de Ciència de Materials de Barcelona (ICMAB-CSIC), Campus UAB, 08193 Bellaterra, Spain

(Received 11 December 2010; published 29 March 2011)

Macroscopically, confined electron gases at polar oxide interfaces are rationalized within the simple "polar catastrophe" model. At the microscopic level, however, many other effects such as electric fields, structural distortions and quantum-mechanical interactions enter into play. Here, we show how to bridge the gap between these two length scales, by combining the accuracy of first-principles methods with the conceptual simplicity of model Hamiltonian approaches. To demonstrate our strategy, we address the equilibrium distribution of the compensating free carriers at polar $LaAlO_3/SrTiO_3$ interfaces. Remarkably, a model including only calculated bulk properties of $SrTiO_3$ and no adjustable parameters accurately reproduces our full first-principles results. Our strategy provides a unified description of charge compensation mechanisms in $SrTiO_3$-based systems.

DOI: 10.1103/PhysRevLett.106.136803 PACS numbers: 73.20.−r, 71.15.−m, 71.70.−d

The unusual behavior of the (001) $LaAlO_3/SrTiO_3$ interface is commonly understood in terms of the "polar catastrophe" (PC) model. [1] By stacking charged $(LaO)^+$ and $(AlO_2)^-$ layers on top of the charge-neutral TiO_2 and SrO layers, one obtains a net interface charge density of $\sigma_{PC} = +e/2S$, where S is the unit-cell cross section. This produces a diverging electrostatic energy, unless σ_{PC} is neutralized by an external free charge, which explains the appearence of confined mobile carriers at this interface. This model, while appealing, misses many important effects, that are crucial for a realistic description of the interface. For example, it was shown that strong polar distortions in $LaAlO_3$ [2] and/or in $SrTiO_3$ [3,4] partially screen the excess charge, delaying the onset of metallicity far beyond what the PC arguments would predict. Next, it was shown that H adsorbates [5] or oxygen vacancies [6] at the open LAO surface can profoundly alter the sheet density of free carriers. Moreover, reversible metal-insulator transitions upon application of an external bias were also demonstrated [7,8]. All these effects go clearly beyond the oversimplified PC description. Finally, the PC model cannot predict truly *microscopic* properties of the system, such as the spatial decay and confinement of the free electrons near the interface. In an attempt to address these latter issues, a number of quantum-mechanical explanations were proposed [9,10], but their relative importance, especially in relationship to the macroscopic electrostatics arguments, is unclear. In this Letter we show how to rationalize these many ingredients into a unified model, where the respective role of the electrostatic and quantum-mechanical effects are unambiguously identified.

We start our derivation by briefly reviewing the theory of "polar discontinuities" that was developed in Ref. [3]. The strategy is based on the *formal* [11] definition of the polarization, P, in quantum-mechanical systems, which has a simple classical interpretation in terms of a point-charge model (see Fig. 1). The dipole moment of an individual $(LaO) - (AlO_2)$ unit is $d = -ea/2$ [black arrows in Fig. 1(b)], where a is the out-of-plane lattice parameter and e is the (positive) electronic charge. This corresponds to a "built-in" polarization $P^0_{LAO} = -e/2S$, where S is the cell surface. Conversely, $P^0_{STO} = 0$ because the STO layers are formally charge-neutral. Note that there is no leftover ionic charge at the interface—we have reinterpreted σ_{PC}, as a surface density of *bound* charge, that arises because of a discontinuity in P.

Depending on the electrical boundary conditions, macroscopic electric fields, respectively $\mathcal{E}_{LAO}$ and $\mathcal{E}_{STO}$, will be present on one or either side of the junction. The electric fields will in turn perturb the individual LAO and STO layers, producing an "induced" polarization that we call ΔP_{LAO} and ΔP_{STO}. If we now define the total polarization as $P = P^0 + \Delta P$, and the electric displacement as $D = \epsilon_0 \mathcal{E} + P$, an *exact* relationship follows,

$$D_{LAO} - D_{STO} = \sigma_{free}, \tag{1}$$

where σ_{free} is a surface density of "free" charge confined to the interface region. Equation (1) generalizes the theory of

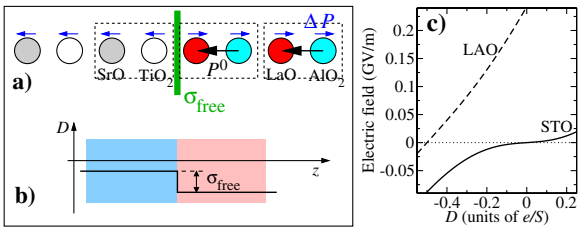

FIG. 1 (color online). (a) Scheme of the TiO_2: LaO interface, showing the built-in (P^0, black arrows) and induced (ΔP, blue arrows) polarization, and the free charge σ_{free}. (b) Electric displacement as a function of z, illustrating Eq. (1). (c) Calculated internal electric fields $\mathcal{E}$ in bulk STO and LAO as a function of D. The polar nature of the interface stems from the impossibility of finding a common value of D for which $\mathcal{E}_{LAO}$ and $\mathcal{E}_{STO}$ are both zero.

Ref. [3] to the case of a nonzero $\sigma_{\rm free}$. This formulation goes beyond the PC model, as it takes rigorously into account the effect of polar distortions (ΔP is implicitly contained in D), external biases [$\mathcal{E}(D)$ is a bulk property of either material, and is a unique function of D, see Fig. 1(c)] and charged species adsorbed on the far-away surfaces (the flux of D corresponds to the surface charge density). By appropriately choosing the two independent parameters $D_{\rm LAO}$ and $D_{\rm STO}$ one can therefore describe the local properties of an ideal interface within arbitrary boundary conditions, encompassing virtually all theoretical approaches (stoichiometric or nonstochiometric superlattices and various flavors of slab geometries, see Ref. [12], Sec. 4) that were used so far in the literature [13,14]. One does not need to worry about the specific mechanisms and/or supercell geometries that determine a certain equilibrium value of $D_{\rm LAO}$ and $D_{\rm STO}$, as long as the interface can be thought as isolated (say, separated by at least two or three unit cells of LAO and STO on either side).

To work our way towards the microscopics, it is now tempting to take the analogy to macroscopic Maxwell equations one step further, and write

$$\frac{dD(z)}{dz} = \rho_{\rm free}(z). \tag{2}$$

Here, $\rho_{\rm free}(z)$ is the spatially resolved planar average of free carriers, whose integral along z yields $\sigma_{\rm free}$. It is easy to verify that Eq. (2) is consistent with Eq. (1). Here one runs into trouble, however, as one needs to establish a truly *microscopic* definition of both $D(z)$ and $\rho_{\rm free}$. [This was not necessary at the level of Eq. (1), which deals only with macroscopic quantities.] This is a nontrivial issue in a typical metal, where the polarization (and hence D) is ill defined. Furthermore, $\rho_{\rm free}$ is microscopically difficult to identify, as the bands corresponding to the conduction electrons are generally entangled with lower-lying bound states. In a doped oxide or semiconductor, however, the valence and conduction bands usually preserve their identity; i.e., a well-defined energy gap persists between conduction-band and valence-band states. This naturally leads to a definition of $\rho_{\rm free}$ based on the overall density of the partially occupied states near the Fermi level. The remainder is an *integer* number of electrons that we identify as bound charges. We use these latter orbitals to define a layer-resolved electric displacement, based on a Wannier decomposition of the polarization, [3,15] in analogy with standard insulators (see Ref. [12], Sec. 3).

We are now ready to verify Eq. (2) directly on our first-principles calculations. To provide a representative number of test cases, we study three combinations of $D_{\rm STO}$ and $D_{\rm LAO}$, which are summarized in the insets of Fig. 2. Case (a) corresponds to full compensation, e.g., that of a thick LAO overlayer on a thick STO substrate. Case (b) corresponds to partial compensation, which can occur at intermediate LAO thicknesses [16], or in the case of an electrical bias applied between the electron gas and an electrode deposited on the free surface.

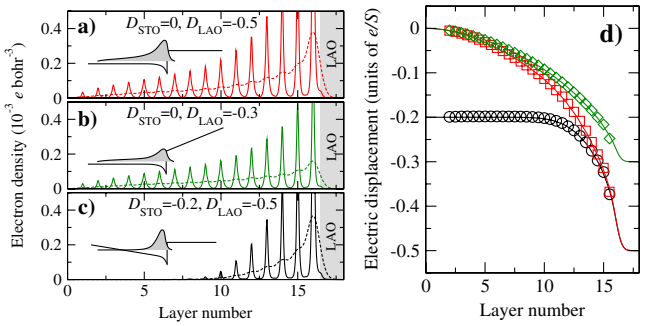

FIG. 2 (color online). Conduction charge (a)–(c) and local electric displacement (d) at the $SrTiO_3/LaAlO_3$ interface. In (a)–(c) the solid curves are $\rho_{\rm free}(z)$ and the dashed curves are the nanosmoothed $\bar{\rho}_{\rm free}(z)$. Insets show an approximate diagram of the effective local potential and $\bar{\rho}_{\rm free}$ (shaded areas). In (d) the symbols show the Wannier-based local electric displacement computed from the bound charges. The curves represent $\int_{\infty}^{z} \bar{\rho}_{\rm free}(t)dt + D_{\rm STO}$.

Case (c) physically corresponds to a ''back-gating'' regime, where an electrical bias is applied between the electron gas and an electrode placed at the other end of the STO substrate. In practice, we use slab geometries of the type vacuum/$(SrTiO_3)n/(LaAlO_3)m$/vacuum (we use $n = 16$ and $m = 3$ in our calculations), where the boundary conditions on D are enforced as explained in the SI, Sec. 2. (All the other relevant computational parameters are also described there; in SI, Sec. 6 we discuss the role of m.) In Fig. 2 we show the relaxed $\rho_{\rm free}(z)$ (a)–(c) and the layer-by-layer (locally averaged) electric displacement D_l (d) for each combination. In Fig. 2(d) we also plot three curves that we constructed by numerically integrating the nanosmoothed charge densities, $\bar{\rho}_{\rm free}(z)$. [We are therefore verifying the integral version of Eq. (2), $D(z) = \int_{-\infty}^{z} \bar{\rho}_{\rm free}(t)dt + D(-\infty)$.] The matching is excellent in all cases, demonstrating the high accuracy of Eq. (2). Note that in one of the examples (case c) $\rho_{\rm free}$ decays to zero relatively fast when moving away from the interface, while it spreads over the whole volume of the $SrTiO_3$ film in the other two cases. This is due to the fact that in (c) the asymptotic electric field in STO is not zero, but equal to $\mathcal{E}(D = -0.2) \sim -12$ MV/m [see Fig. 1(c)]. This produces a confining wedge potential, that limits the spread of $\rho_{\rm free}$. Conversely, in (a) and (b), $\mathcal{E}$ vanishes at $z \longrightarrow -\infty$, and the outermost electrons are only loosely bound.

Equation (2) is an important result, in that it establishes a direct, virtually exact relationship between the density of compensating carriers and the local polarization [note that $P(z) \sim D(z)$] in LAO and STO. This answers pressing experimental questions concerning precisely this point, as polar distortions in $SrTiO_3$ were recently observed [17]. This also has profound implications over the theoretical understanding of electron confinement in this system, as we shall demonstrate in the following.

Essentially, the equilibrium distribution of the conduction charge is determined by two competing effects. One is

the electrostatic energy, that tends to localize the electrons as close to the interface as possible. The strength of the attraction depends on the static dielectric constant of the underlying insulator (see Ref. [12], Sec. 5). The other is the quantum-mechanical kinetic energy of the electrons. This tends to spread the electrons in space, with a strength that depends on the band dispersion. To see whether, and to what extent, the large polar distortions in STO affect these competing driving forces, we performed calculations (see Ref. [12], Sec. 2.2) of bulk $SrTiO_3$ as a function of the electric displacement [18], by covering the range of D_{STO} values that are relevant for the LAO/STO system. For each value of D we extract the built-in electric field, the total internal energy and the relevant parameters of the lower part of the conduction band. These are the tight-binding hopping integrals between Ti-derived orbitals with t_{2g} symmetry (d_{xy}, d_{xz} and d_{yz}). As the t_{2g} orbitals are fairly well localized in space, it is sufficient for the present study to consider only the first three shells of nearest-neighbor Ti sites.

In Fig. 3(a) we show the electric field as a function of the displacement field D. Note the strong nonlinearity in the dielectric constant as a function of D [Fig. 3(b)]. In Fig. 3(c) we show the band structure as it results from the third-neighbor Hamiltonian, for the centrosymmetric cubic state at $D = 0$. Note the symmetry of the bands, which are characterized by a threefold degeneracy at Γ. A polarization [the extreme case $D = -e/2S$ is shown in Fig. 3(d)] lifts this degeneracy, by producing a strong splitting at Γ between the degenerate d_{xz}/d_{yz} orbitals and the d_{xy} orbital. This splitting is dominated by the reduction in the d_{xz}/d_{yz} bandwidth along the $\Gamma \rightarrow X$ and $\Gamma \rightarrow Z$ directions by 30% and 25%, respectively.

We shall now use these data to develop a quantitative model of the equilibrium distribution $\rho_{\mathrm{free}}(z)$. We make a rather bold assumption here, and state that the role played by the $LaAlO_3$ overlayer in determining $\rho_{\mathrm{free}}(z)$ is marginal, except for two crucial effects: (i) it confines the conduction electrons to the STO side, and (ii) it defines the electrical boundary conditions through the value of D_{LAO}. Based on this *ansatz*, we represent the LAO/STO interface systems discussed in the previous paragraphs as *pure* STO slabs, periodic in plane and n-layer thick, where the boundary values of the electric displacement field at the two surfaces are set to D_{STO} and D_{LAO}. To each Ti site l we assign three orbitals of t_{2g} symmetry, and a charge density ρ_l. The charge density defines the local value of the electric displacement D_l through Eq. (2). The Hamiltonian matrix elements are defined by the electrostatic potential V_l [calculated from D_l using the bulk $V_{\mathrm{STO}}(D)$ of Fig. 3(a)], which rigidly shifts the on-site terms, and by the D_l-dependent hopping parameters that we interpolate from the bulk $SrTiO_3$ data. Upon diagonalization we obtain the wavefunctions, that self-consistently determine ρ_l within the constraint Eq. (1).

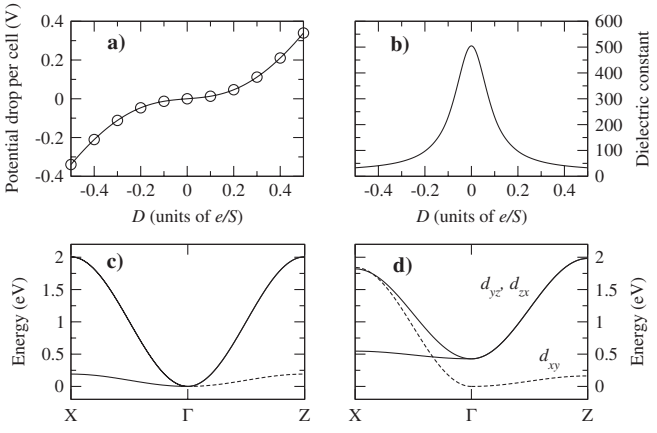

FIG. 3. Bulk properties of $SrTiO_3$ used in the tight-binding model. Upper panels: internal potential (a) and dielectric constant (b) as a function of D. Lower panels: t_{2g} conduction-band structure for $D = 0$ (c) and $D = -e/2S$ (d).

In Fig. 4 we compare the results of the model to the first-principles simulations discussed earlier. We include in the comparison a fourth simulation that we did for case $D_{\mathrm{STO}} = 0$, $D_{\mathrm{LAO}} = -e/2S$, but with a thicker STO layer ($n = 24$). The agreement is remarkably good. This indicates that the D-dependent bulk properties of $SrTiO_3$, together with the boundary values of D, are sufficient to explain the distribution of conduction charge in this system. This suggests that the interaction between Ti- and La-derived orbitals is not an essential factor in determining electron confinement, contrary to the conclusions of

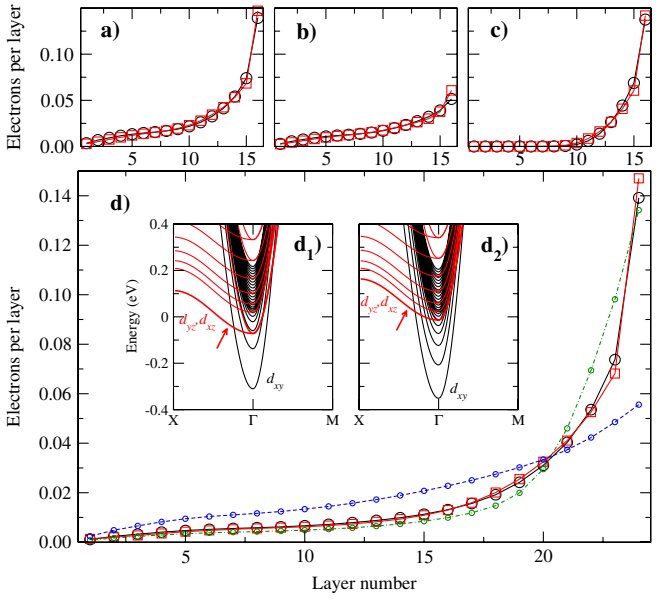

FIG. 4 (color online). Electron confinement and spatial distribution. Red curves with square symbols are the first-principles results, black curves (circles) are the results of the model. Parameters are the same as in Figs. 2(a)–2(c). (d) shows a thicker 24-cell STO film. The dashed (blue) and dot-dashed (green) curves were obtained by artificially altering selected features of the model (see text). Insets: tight-binding band structures corresponding to the green (d_1) and black (d_2) curves in (d). The arrow indicates the lowest d_{yz}/d_{zx} state.

Ref. [9]. Binding of the electrons to the interface is indeed guaranteed by Eq. (2) (see Ref. [12], Sec. 5).

Now that we have a reliable model we can directly quantify the impact of each specific STO bulk property on the distribution of ρ_{free}. First, if we neglect the nonlinearity in the dielectric permittivity $\epsilon_{\text{STO}}(D)$, and instead use a constant $\epsilon_{\text{STO}}(D) = \epsilon_{\text{STO}}(0) \sim 500$ we obtain a much broader distribution [blue curve in Fig. 4(d)]. This indicates that the carrier distribution is strongly sensitive to the dielectric properties of bulk STO; this seems to be an accepted fact in the experimental community, [19] but has received surprisingly little attention in earlier *ab initio* studies. Second, if we suppress the D dependence of the STO band structure, and use the $D = 0$ t_{2g} Hamiltonian throughout the film, we obtain [green curve in Fig. 4(d)] an excessive accummulation of charge in the near-interface region. This effect can be understood by comparing the self-consistent band structures of the original [Fig. 4 (d_2)] and the "$t_{2g}(D = 0)$" [Fig. 4 (d_1)] tight-binding models. In both cases there is a strong splitting at Γ between the d_{xy} and d_{xz}/d_{yz} bands, in agreement with the findings of Refs. [14,16,20]. In Fig. 4 (d_1), however, this splitting is only induced by *confinement* effects due to the wedgelike electrostatic potential near the interface [21]. The polarization-induced perturbations in the STO t_{2g} bands [Fig. 3(d)] enhance such a splitting [Fig. 4 (d_2)] and shift the d_{xz}/d_{yz} bands further up in energy. (The effect is strongest on the lowest d_{xz}/d_{yz} band, marked with a red arrow in the figure.) This upshift, in turn, pushes the weight of the d_{xz}/d_{yz} electrons away from the LAO interface, which explains the difference between the respective electron distributions [green and black curves in Fig. 4(d)]. Note that an analogous t_{2g} splitting was experimentally observed in LAO/STO, [22] and theoretically also discussed in the context of the closely related $LaTiO_3/SrTiO_3$ system [23].

The tight-binding method used here has clear points of contact with the strategy of Refs. [23,24]. However, in our approach there is a crucial innovation. Here, at difference with Ref. [23], we extract all the ingredients of the model from *bulk* calculation of pure insulating $SrTiO_3$, without including any adjustable parameter. This forces us to build a universal and transferable model, which can be readily applied to essentially any situation involving electrostatic doping of $SrTiO_3$, and is not restricted to the specifics of the $LaAlO_3/SrTiO_3$ interface. For example, our strategy could be readily used, with little modifications, to interpret the recent findings of electron gases at the bare $SrTiO_3$ surface [21]. More importantly, our model could be readily extended to account for other physical ingredients not considered here, e.g., strong correlations [13] and strain effects; [25] one just needs to refine the theoretical description of bulk STO that is provided as an input. This is an enormous advantage, both conceptually (the model is based on few parameters that are easy to interpret) and practically (the tight-binding model is several orders of magnitude more efficient than a full first-principles calculation). More generally, our results open exciting new avenues for the study of confined electron gases in oxide systems, with optimal accuracy and dramatically reduced computational cost.

I wish to thank G. Herranz, J. Íñiguez, and Ph. Ghosez for their careful reading of the manuscript. This work was supported by MICINN-Spain (Grants No. MAT2010-18113 and No. CSD2007-00041, and the Ramón y Cajal program) and the EC-FP7 project OxIDes (Grant No. CP-FP 228989-2). Computing time was kindly provided by BSC-RES and CESGA.

*mstengel@icmab.es

[1] A. Ohtomo and H. Y. Hwang, Nature (London) **427**, 423 (2004).
[2] R. Pentcheva and W. E. Pickett, Phys. Rev. Lett. **102**, 107602 (2009).
[3] M. Stengel and D. Vanderbilt, Phys. Rev. B **80**, 241103 (2009).
[4] N. C. Bristowe, E. Artacho, and P. B. Littlewood, Phys. Rev. B **80**, 045425 (2009).
[5] W.-J. Son, E. Cho, J. Lee, and S. Han, J. Phys. Condens. Matter **22**, 315501 (2010).
[6] C. Cen, S. Thiel, J. Mannhart, and J. Levy, Science **323**, 1026 (2009).
[7] C. Cen *et al.*, Nature Mater. **7**, 298 (2008).
[8] S. Thiel, G. Hammerl, A. Schmehl, C. W. Scheneider, and J. Mannhart, Science **313**, 1942 (2006).
[9] H. Chen, A. Kolpak, and S. Ismail-Beigi, Phys. Rev. B **82**, 085430 (2010).
[10] K. Janicka, J. P. Velev, and E. Y. Tsymbal, Phys. Rev. Lett. **102**, 106803 (2009).
[11] R. Resta and D. Vanderbilt, in *Physics of Ferroelectrics: A Modern Perspective*, edited by K. M. Rabe, C. H. Ahn, and J.-M. Triscone (Springer-Verlag, Berlin, Heidelberg, 2007).
[12] See supplemental material at http://link.aps.org/supplemental/10.1103/PhysRevLett.106.136803.
[13] R. Pentcheva and W. E. Pickett, J. Phys. Condens. Matter **22**, 043001 (2010).
[14] H. Chen, A. M. Kolpak, and S. Ismail-Beigi, Adv. Mater. **22**, 2881 (2010).
[15] X. Wu, O. Diéguez, K. M. Rabe, and D. Vanderbilt, Phys. Rev. Lett. **97**, 107602 (2006).
[16] W.-J. Son, E. Cho, B. Lee, J. Lee, and S. Han, Phys. Rev. B **79**, 245411 (2009).
[17] N. Ogawa *et al.*, Phys. Rev. B **80**, 081106 (2009).
[18] M. Stengel, N. A. Spaldin, and D. Vanderbilt, Nature Phys. **5**, 304 (2009).
[19] O. Copie *et al.*, Phys. Rev. Lett. **102**, 216804 (2009).
[20] Z. S. Popović, S. Satpathy, and R. M. Martin, Phys. Rev. Lett. **101**, 256801 (2008).
[21] A. F. Santander-Syro *et al.*, Nature (London) **469**, 189 (2011).
[22] M. Salluzzo *et al.*, Phys. Rev. Lett. **102**, 166804 (2009).
[23] S. Okamoto, A. J. Millis, and N. A. Spaldin, Phys. Rev. Lett. **97**, 056802 (2006).
[24] S. Okamoto and A. J. Millis, Nature (London) **428**, 630 (2004).
[25] C. W. Bark *et al.*, Proc. Natl. Acad. Sci. U.S.A. **108**, 4720 (2011).